



OPEN

Analysis of the Breakthrough Listen signal of interest blc1 with a technosignature verification framework

Sofia Z. Sheikh¹✉, Shane Smith^{1,2}, Danny C. Price^{1,3}, David DeBoer⁴, Brian C. Lacki¹, Daniel J. Czech¹, Steve Croft^{1,5}, Vishal Gajjar¹, Howard Isaacson^{1,6}, Matt Lebofsky¹, David H. E. MacMahon^{1,4}, Cherry Ng^{1,5,7}, Karen I. Perez⁸, Andrew P. V. Siemion^{1,5,9}, Claire Isabel Webb^{1,10}, Andrew Zic^{11,12}, Jamie Drew¹³ and S. Pete Worden¹³

The aim of the search for extraterrestrial intelligence (SETI) is to find technologically capable life beyond Earth through their technosignatures. On 2019 April 29, the Breakthrough Listen SETI project observed Proxima Centauri with the Parkes ‘Murriyang’ radio telescope. These data contained a narrowband signal with characteristics broadly consistent with a technosignature near 982 MHz (‘blc1’). Here we present a procedure for the analysis of potential technosignatures, in the context of the ubiquity of human-generated radio interference, which we apply to blc1. Using this procedure, we find that blc1 is not an extraterrestrial technosignature, but rather an electronically drifting intermodulation product of local, time-varying interferers aligned with the observing cadence. We find dozens of instances of radio interference with similar morphologies to blc1 at frequencies harmonically related to common clock oscillators. These complex intermodulation products highlight the necessity for detailed follow-up of any signal of interest using a procedure such as the one outlined in this work.

From 2019 April 29 to May 4, the Breakthrough Listen (BL) project performed observations to place limits on the prevalence of radio technosignatures (non-human ‘objects, substances, and/or patterns whose origins specifically require a [technological] agent’, by analogy with biosignatures¹) in the direction of Proxima Centauri (ProxCen). ProxCen is an astrobiologically fascinating target due to its proximity: it is the closest star to the Sun at 1.295 pc (ref. ²); it is host to Proxima b, the closest known exoplanet to the Earth^{3,4}, which lies in the traditional habitable zone of ProxCen; and it has even featured as the target of a proposed in situ search via Breakthrough Starshot⁵.

We employed the Commonwealth Scientific and Industrial Research Organisation (CSIRO) Parkes ‘Murriyang’ telescope with the Ultra-Wideband Low receiver (UWL)⁶, across 0.704–4.032 GHz, as part of the project ‘P1018: Wide-band radio monitoring of space weather on Proxima Centauri’ (primary investigator A.Z.). These observations were part of an international multi-wavelength campaign to monitor ProxCen for stellar flares⁷, collaboratively carried out using the BL Parkes Data Recorder backend in shared-risk mode^{8,9}. In parallel with the P1018 flare search, the BL team used the data to conduct a technosignature search of ProxCen. Over those six days, ProxCen was observed for a total of 26 h 9 min; data are available at seti.berkeley.edu/blc1.

We searched for narrowband drifting signals in high-resolution dynamic spectra¹⁰ with ~17 s subintegrations and ~4 Hz frequency

resolution. We ran the turboSETI version 1.2.2 (turbo search for extraterrestrial intelligence) narrowband search algorithm, as described in a companion paper¹¹, and the pipeline returned a narrowband event that appeared in two consecutive observations of ProxCen and did not appear in any reference ‘off-source’ observations towards astronomical calibrator sources between the ‘on-source’ ProxCen observations, even upon visual inspection. This single event was named ‘blc1’ as shorthand for ‘Breakthrough Listen candidate 1’. We find ‘signal of interest’ to be a more appropriate categorization than ‘candidate’ (see, for example, ref. ¹² and Supplementary Discussion 1.1), but as ‘blc1’ is already in common usage, we will continue to use it here. The blc1 signal is shown in Fig. 1 and its properties are enumerated in Table 1.

The blc1 signal is intriguing because:

1. It is a ~Hz-wide narrowband signal, which cannot be created by any known or foreseeable astrophysical system, only by technology¹³.
2. It exhibits a non-zero drift rate, as expected for a transmitter that was not on the surface of the Earth.
3. Its drift rate appears approximately linear in each 30 min ‘panel’ (one single-target observation from a cadence of observations that makes up a waterfall plot such as Fig. 1), but the drift rate changes smoothly over time, as expected for a transmitter in a rotational/orbital environment.

¹Department of Astronomy, University of California Berkeley, Berkeley, CA, USA. ²Department of Physics, Hillsdale College, Hillsdale, MI, USA.

³International Centre for Radio Astronomy Research, Curtin University, Bentley, WA, Australia. ⁴Radio Astronomy Laboratory, University of California Berkeley, Berkeley, CA, USA. ⁵SETI Institute, Mountain View, CA, USA. ⁶Centre for Astrophysics, University of Southern Queensland, Toowoomba, Queensland, Australia. ⁷Dunlap Institute for Astronomy and Astrophysics, University of Toronto, Toronto, Ontario, Canada. ⁸Department of Astronomy, Columbia University, New York, NY, USA. ⁹Department of Physics and Astronomy, University of Manchester, Manchester, UK. ¹⁰Berggruen Institute, Los Angeles, CA, USA. ¹¹Department of Physics and Astronomy, and Research Centre in Astronomy, Astrophysics and Astrophotonics, Macquarie University, Macquarie Park, New South Wales, Australia. ¹²Australia Telescope National Facility, CSIRO Space and Astronomy, Epping, New South Wales, Australia. ¹³Breakthrough Initiatives, NASA Research Park, Moffett Field, CA, USA. ✉e-mail: ssheikh@berkeley.edu

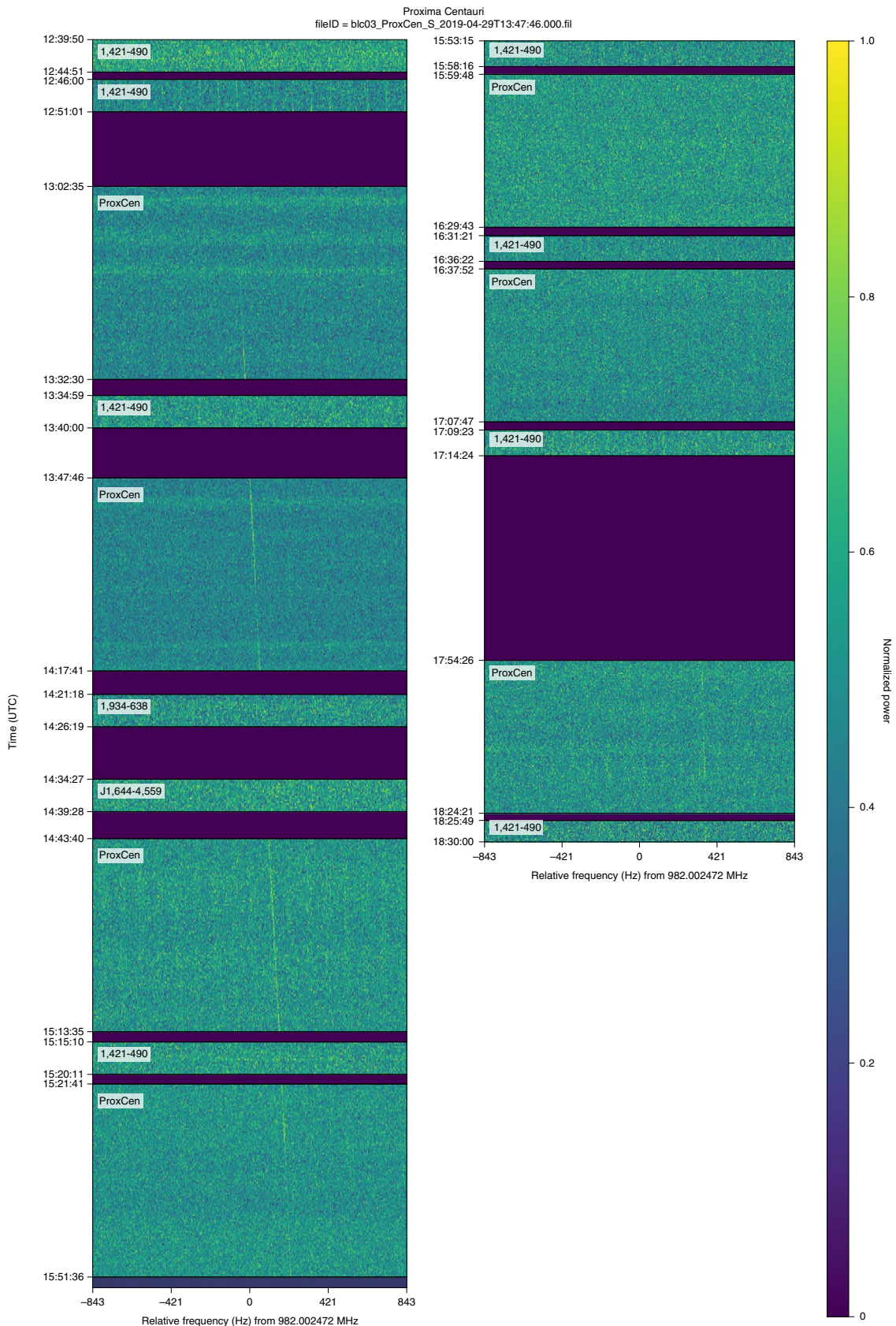


Fig. 1 | A waterfall plot (dynamic spectrum) around 982 MHz depicting alternating observations of ProxCen and off-source positions from 2019 April 29. The horizontal axis shows the relative frequency offset from a start frequency, the y axis shows time progressing from top to bottom (and from left to right, continuing from the end of the first column to the beginning of the second) and the colour bar shows detected power (linearly normalized). The blc1 signal is visible as the diagonal linear feature in ProxCen panels 1, 2, 3, 4 and 7. Data were not taken during the periods marked by purple panels, which are primarily telescope slews.

Table 1 | Basic characteristics of blc1

Characteristic	Value
Detection date	2019 April 29
Time at first detection	13:17:35.232 UTC
Time at last detection	18:19:26.400 UTC
Length of persistence	5.03 h
Signal frequency at first detection	982.0024 MHz
Signal frequency at last detection	982.0028 MHz
Initial drift rate	0.0326 Hz s ⁻¹
Average signal-to-noise ratio ^a	17.956
Signal bandwidth	<3.81 Hz

^a Average signal-to-noise ratio is calculated as the average of the signal-to-noise ratios from the five 30 min observations in which blc1 appeared.

- It is absent in the off-source observations (see ‘Initial investigation and parametrization of blc1’), as expected for a signal that is localized on the sky.
- It persists over several hours, making it unlike other interferers from artificial satellites or aircraft that we have observed before.

For these reasons, especially Point 4 (by which we have ruled out turboSETI outputs in previous searches, for example, in ref. ¹⁴), blc1 warranted an in-depth analysis beyond any event so far in the course of the BL initiative.

Initial investigation and parametrization of blc1

We first ensured that the telescope and backend logs showed normal operation, mapped out the telescope pointings against the local site and checked that the data recording was functioning correctly. Upon consultation with the observatory and the Australian Communications and Media Authority, we found that there is no catalogued radio-frequency interference (RFI) at the Parkes Observatory at 982.002 MHz, nor registered transmitters at that frequency in Australia. The band near 982 MHz is more broadly reserved for aircraft.

A signal that is truly localized on the sky should be detected only when the telescope is pointed at that location, if the off-source positions are suitably chosen with regard to the sidelobe pattern of the telescope. To ensure that the behaviour seen in the off-source observations is consistent with a localized emitter in the on-source, we must consider the cadence, off-source positions and off-source luminosities, and perform a thorough search for highly attenuated power on the off-source observations. The ProxCen campaign employed a modified observing strategy that was different than the usual BL procedures^{14,15}, to fulfil the project’s primary goal, which was to observe and characterize stellar flares from ProxCen. The cadence was non-standard, consisting of 30 min integrations on ProxCen that alternated with 5 min observations of the calibrators. This cadence was chosen to maximize the on-source time. However, the asymmetry in the observing lengths (30 min versus 5 min) causes an associated asymmetry in the expected signal-to-noise ratio (S/N) from the same signal in a turboSETI analysis by a factor of $\sqrt{\frac{30}{5}}$.

In addition, the off-source positions were two quasars (and a single pulsar, observed once) selected from the Australia Telescope National Facility calibrator database. Off-sources for turboSETI are usually chosen to be positions, usually stars, without a detectable radio flux, for consistency when evaluating apparent S/Ns between on-sources and off-sources. As these observations were being used for flare detection, the off-sources were chosen as quasars for frequent evaluation of the system temperature. The quasars, given

their intrinsic radio emission, have a higher ‘noise floor’ that we must contend with when searching for narrowband emission. From ref. ¹⁶, we find a flux of $S(\nu) = 10$ Jy at a frequency ν of 982 MHz for both PKS 1421-490 and PKS 1934-638. Given our system equivalent flux density of ~ 38 Jy from above, this leads to a total flux density of 48 Jy when observing on a calibrator.

Finally, the off-source positions were significantly farther from ProxCen than in a normal BL observation. PKS 1421-490 is 12.57° from ProxCen and PKS 1934-638 is 45.82°. These distances led to the long slew times shown in Fig. 1, which can cause the temporal RFI environment to change between the on-source and off-source observations. There may also be a large spatial difference in directional RFI, especially when complicated by the telescope sidelobes. Similarly, the position of ProxCen changed in sky coordinates by 30°, primarily in azimuth, from first detection to final detection.

In this case, the first two effects would downweight the expected S/N of blc1 in the off-source observations by a factor of $\sqrt{\frac{30}{5}} \times \frac{48}{38} \approx 3$, which should still be detectable in a de-drifted sum if

the signal were present in the off-source. We took all nine off-source panels in Fig. 1 and individually examined their waterfall plots, confirming that there was no visible signal in the first eight. The ninth and final off-source shows some power near 982.0028 MHz.

Highly attenuated signals in an off-source observation may become apparent only after removing the expected drift rate. To this end, we de-drifted each off-source panel to the nearest best-fit drift rates (Supplementary Methods 2.1). The final off-source does show a faint narrowband signal (S/N < 5), but the best-fit drift rate for this signal is 0 Hz s⁻¹, not 0.14 Hz s⁻¹. Although this could be interpreted as blc1 appearing in an off-source, we deemed it inconclusive given the lack of appearance in the previous off-source observations, the known presence of a 0 Hz s⁻¹ interference comb in the spectrum (see ‘Frequency comb’), the mismatch of the expected and measured drift rate, and the low S/N.

Finally, to search for constant, highly attenuated power across the off-sources, the panels can be individually summed across their 5 min and 30 min lengths to create integrated spectra, and those spectra can in turn be summed to produce an incoherent sum across every off-source observation. We saw no resulting signal (S/N ≥ 5) in the de-drifted spectra of any non-detection, nor any signal in the incoherent sum of the nine off-sources. This indicates that either the phenomenon was localized on the sky (either near ProxCen’s location or near a source in the sidelobes of the telescope) or the phenomenon had a duty cycle or brightness variation that matched our chosen cadence particularly well.

Frequency comb. Using an auto-correlation function in frequency, we find evidence for an RFI frequency comb, which is a set of non-drifting signals regularly spaced in frequency with stable amplitude, in the blc1 observation (Supplementary Fig. 16).

The comb is present in the on-sources and the off-sources, has a spacing of ~ 80.1 Hz and is present throughout the entire 128 MHz sub-band, from 960 to 1,087 MHz. This implies that the comb is not localized to the part of the spectrum around blc1, lowering the likelihood that they are related phenomena. To investigate this further, we searched for reappearances of the frequency comb in other UWL observations (using the 7,000 observation data set described in ‘Other Murriyang signals near 982 MHz’) and found that the comb appeared occasionally, throughout the year, without any associated signals at 982 MHz. We did not detect the frequency comb in any of the 2020 November or 2021 April re-observations (see ‘Re-observations’).

We deem the comb to be independent of blc1 based on observing the comb over the week of ProxCen observations and in unrelated campaigns throughout the year in both on and off-sources (indicative of RFI) without an appearance of blc1, on the lack of drift in the frequency comb, and on a lack of correlation between the S/N over

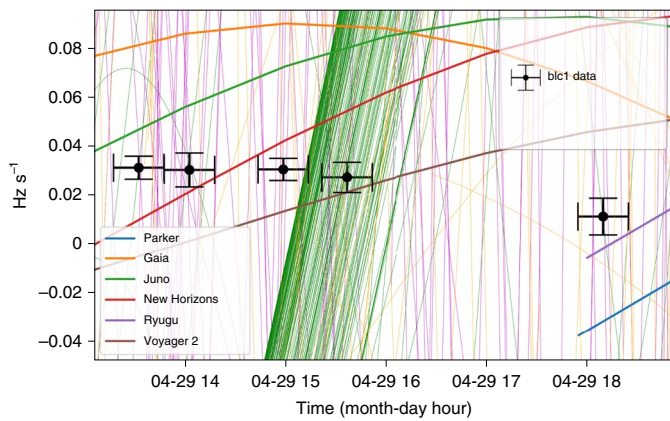


Fig. 2 | Drift characteristics of non-LEO satellites and deep-space probes above the horizon during the event time. The green thin lines are GEO, the magenta are MEO and the orange are other non-LEO satellites. The thick lines are deep-space probes: Parker Solar Probe (blue), Gaia (orange), Juno (green), New Horizons (red), Ryugu (purple) and Voyager 2 (brown). The black data points show the b1c1 data (Supplementary Table 1), where the x-axis bars are the time of observation and the y-axis bars are 1σ error bars. The deep-space probes are closer to the correct order of b1c1's drift due to their unique status as near-sidereal sources, but none can explain b1c1.

time of the comb and the S/N over time of the signal. However, the RFI comb unfortunately complicates the measurement of parameters, especially the S/N, in observations of signals similar to b1c1 with heavy interference.

Re-observations. Around 2020 mid-November, we began to re-observe ProxCen during our scheduled observation time at Murriryang, for sessions when it was above the horizon. We re-observed ProxCen on November 19, 26 and 30, for 3–4 h on each occasion. These re-observations were performed with the same UWL receiver, BL backend and outputted data product as the original observation of b1c1. However, we chose a more standard cadence for the re-observations, 15 min on-source on ProxCen and 15 min off-source, with the off-sources chosen to be nearby stars at different relative angles to the ProxCen–ground vector. No signals of any drift rate were detected at $\nu_{\text{b1c1}} \pm 2$ kHz in any of these three re-observations.

Two years after the original detection, from 2021 April 29 to May 3, we observed for 12 h each day to replicate the relevant portion of the initial ProxCen session in 2019. These re-observations were performed with the same UWL receiver, BL backend, outputted data product, local time and cadence as the original observation of b1c1. No signals of any drift rate were detected at $\nu_{\text{b1c1}} \pm 2$ kHz in any of these re-observations.

Constraining physical and electronic drift rates

Signals drifting in frequency are generated in one of two ways: a transmitter accelerating relative to the observer, or an electronically varying (deliberately or not) transmitter. Both means may be present at any given time.

Strong ground-based RFI entering into a distant sidelobe may remain detectable even when the telescope is pointed at different parts of the sky. The sidelobe may downweight the signal by a factor of 10^5 (50 dB) or more⁶, but the signal may still be detected with higher S/N than an intrinsically weak and/or distant signal coming through the main lobe with as little as one millionth of the flux density. For satellites, the main lobe and near-in sidelobes subtend a very small area, so ‘direct hits’ from satellites are rare but can saturate the receiver when they do occur.

Accelerational drifts. For this analysis, we assume that the signal from a transmitter near 982 MHz is leaking in through either a distant antenna sidelobe or the main beam. We seek to explain both the drift morphology of the signal and the prevalence over a sufficient length of time.

With the frequency fixed, we looked at drift rate characteristics of transmitters undergoing various ‘normal’ motions. The drift is proportional to the relative line-of-sight acceleration between the receiver and transmitter, which can be produced via a change in speed or relative direction. The drift due to just telescope motion as it tracks an object is $< 10^{-4}\dot{\nu}$, where $\dot{\nu}$ is the signal drift of b1c1, and hence does not explain b1c1's characteristics.

Ground-based and aerial transmitters. A transmitter on the ground may be stationary, or be on a moving platform in the vicinity of the telescope, such as a car, train or other vehicle. In the air, the transmitter could be on a plane, helicopter, drone, balloon or other airborne object. To investigate these hypothetical transmitters, we looked at a range of plausible routes around the observatory (say, for someone walking or biking) and for a range of velocities for vehicles along the nearby highway, as shown in Supplementary Fig. 1, for a fixed frequency transmitter. Similarly, we explored a range of plausible airplane velocities and routes between various cities.

Supplementary Fig. 1 shows the primary issue with all of the local signals described above, namely that speeds high enough to exhibit the correct order of drift do not persist long enough; conversely, for low enough speeds to persist, the drifts are too low. None of the drift characteristics from local signals match the measurement, and it is extremely difficult to construct a continual motion path that could persist as exhibited by the measured signal, even by varying the speed along the route.

Satellite transmitters. Next we considered artificial satellites orbiting the Earth, which are broadly grouped as low-Earth orbit (LEO, ~ 90 min orbits), (2) medium-Earth orbit (MEO, ~ 12 h orbits), and (3) geosynchronous orbit (GEO, ~ 24 h orbits). The short period of LEOs implies that they cannot be responsible for the signal regardless of their drift characteristics, so we did not include LEO satellites in our analysis. Conversely, we do include GEO satellites; GEO is often referred to as ‘geostationary’, implying true zero drift, but even stable GEO satellites generally meander in a figure-of-eight motion. There are a small number of satellites in other orbits as well, which are encompassed by the following analysis.

To investigate these satellites, we downloaded orbital element parameters for all known, active, non-LEO satellites for the date in question (<https://www.space-track.org>). All satellites above the horizon are plotted as the faint lines in Fig. 2. Even for geosynchronous satellites (green lines), the drift characteristics vary too rapidly to explain the signal characteristics.

Transmitters on deep-space probes. Deep-space probes are exploratory spacecraft that do not orbit the Earth, and are the most celestially stationary sources produced by humans. Although their radio emission can be strong relative to celestial sources, their distance generally makes them weak enough that they are not readily detectable unless they happen to be in or near the main beam. To investigate space probes, we obtained positional information from NASA Horizons at <https://ssd.jpl.nasa.gov/horizons.cgi>. Figure 2 shows the drift of space probes above the horizon, although none of them coincide with the main beam of the telescope. Their drifts and positions are inconsistent with those of b1c1.

We also considered—and dismissed—transmitters on asteroids and reflections from Earth-bound radio transmitters off of asteroids in the primary beam as a potential source of b1c1 (Supplementary Methods 2.2).

Electronic drifts. Finally, we considered electronically varying signal generators. A modern signal generator can be programmed to produce any drift rate; there are effectively no constraints, and thus we cannot use this to inform our analysis. However, we can constrain other causes of electronic drift related to the temperature, aging and voltage of the oscillator; all oscillators exhibit some drift with these parameters.

This type of RFI is prevalent, but typically the drifts are too low (very good regulation) or too high and wandering (as in more typical commodity devices) for them to be mistaken for an object moving sidereally. They are also almost always seen in both the off-source pointings as well as the on-source pointing. However, given their prevalence, occasionally a device could potentially exhibit the expected characteristics of a sidereal source, which would be difficult to ascribe to RFI.

Astronomically expected drifts. We can also compare the drift rate magnitude and morphology to the sidereal drift in the direction of ProxCen, as well as known accelerations and orbital periods from the planets in the ProxCen system. Defiance of expectations for drift rates in a target system does not invalidate a signal, but a match provides additional evidence in favour of an interstellar origin. In an effort to be easily detected and discernable as ‘stationary’, a distant transmitter in the direction of the antenna pointing could electronically vary its transmission frequency to compensate for its motion relative to the Sun, the Earth or the barycentre of the Solar System. For the timescales relevant to our observation, the Earth’s rotation is the primary contributor to the expected drift rate for ProxCen, and is similar for all other sidereal sources in the beam (Supplementary Discussion 1.2). Supplementary Fig. 2 shows the relevant geometry of the Earth–Sun–ProxCen positions and the corresponding residual drift. We find that the drift rate of blc1 is not consistent with the barycentric motion expected from the direction of ProxCen, but is consistent with the order-of-magnitude drift that could be produced in the system, based on the orbital and rotational motions of its planets (Supplementary Discussion 1.3).

Searching for other instances of blc1

In parallel with the drift rate analysis, we performed a search for reappearances of the signal of interest on other days and at other frequencies.

Other Murriyang signals near 982 MHz. We searched for signals with the same frequency and same drift as blc1 from both the week-long ProxCen campaign and every archival observation from standard BL Murriyang UWL observing of other stellar targets.

To find all appearances of blc1, even those that were too faint or too masked by RFI to be flagged by turboSETI, we produced output plots for visual inspection from every ProxCen on-source and off-source observation from April 29 to May 4. We restricted the plots to 982.002–982.004 MHz to begin with; a few plots were extended up or down by 1 kHz if there appeared to be interesting behaviour near the upper or lower bounds.

We created and searched two kinds of output plots, namely dynamic time–frequency spectra ‘waterfall’ plots (Fig. 1) and ‘butterfly’ plots, which display the power at each drift-rate–frequency pair after use of a de-drifting algorithm (Supplementary Methods 2.1). Examples of these output plots are shown in Supplementary Fig. 17.

Through analysis of these diagnostic plots, we identified four occurrences of blc1-like signals during the ProxCen observations, which, through their low S/Ns, had failed to reach turboSETI’s detection threshold. An example of one of these similar signals is shown in Fig. 3; the rest are displayed in Supplementary Figs. 3–5.

We performed the same analysis with every archival observation that BL had taken with the Murriyang UWL receiver. In total, this

consisted of about 7,000 observations from 2019 to 2020, primarily nearby stars in the Hipparcos catalogue^{17,18} but also pulsars and quasars used for calibration and, of course, ProxCen. Most of these files had a standard duration of 5 min, as opposed to the 30 min observations from the ProxCen campaign. In many of these observations, we observed the same zero-drift frequency comb as detected in the original blc1 observation (see ‘Initial investigation and parametrization of blc1’), giving more evidence that this comb is unrelated RFI.

We found 15 similar-looking features in these non-ProxCen UWL observations. Visual inspection of the full cadences surrounding these features shows that 14 of them are different from the blc1-like signals in morphology, length, drift behaviour and/or signal strength over time. However, one of the 15 features is clearly RFI due to its persistence across both on-source and off-source observations, appeared four days prior to blc1 and looks to be potentially a member of the set including blc1 and the similar signals from the ProxCen campaign; this signal is shown in Supplementary Fig. 6.

All five of these 982 MHz signals from different days are fainter than blc1; three of them conclusively appear in the off-sources, whereas two of them are inconclusive.

Different frequencies. Human-made communication technologies often use multiple simultaneous frequency channels to send information for improved redundancy and bit rate. It is possible that extraterrestrial intelligence would do the same; it is also possible that the appearance of a blc1 twin at another frequency, if clearly RFI, would allow us to determine that blc1 is also RFI.

To find signals similar to blc1 at different frequencies, we calculated the frequency-normalized drift rate ($\dot{\nu}_{\text{normalized}} = \frac{\dot{\nu}}{\nu}$) that would indicate a signal that was drifting proportionally to blc1 in the first observation. This proportional drift is expected for multi-frequency transmitters in the same accelerational environment, but also in multi-frequency transmitters that are drifting electronically.

We then searched the catalogue of narrowband hits created with turboSETI for signals that appeared at the same time as blc1 and were drifting proportionally in the first panel, plus or minus the drift rate error proxy as given in the first row of Supplementary Table 1. This search returned 112 hits: blc1 itself and 111 signals that turboSETI had identified as hits but then rejected as RFI at an early stage in the pipeline due to their appearance in off-source observations. These hits were plotted in the context of all of the subsequent panels of the ProxCen observation on 2019 April 29.

We visually inspected the 111 matches, looking for signals that had the same morphology as that of blc1 beyond the drift rate in the first panel. To identify a signal with the same morphology, we looked for monotonicity, a shallowing of the slope over time, a vertical length that spanned multiple panels and the absence of complex additional features (for example sinusoidal behaviour). We found that 36 of the 111 turboSETI matches (32%) were blc1 ‘lookalikes’, namely signals with morphology strikingly similar to that of blc1. A subset of these lookalikes is shown in Supplementary Fig. 7, and some examples of the ‘non-lookalikes’ are shown in Supplementary Fig. 8.

The lookalikes have a range of variabilities over time, which seem to indicate multiple transmitters producing unusually consistent drifts. We then performed the same search as before but with negative drift rates. We found 310 hits from RFI, of which 27, upon visual inspection, were found to be mirrored lookalikes, with exactly the same drift structure over time as blc1 but flipped in morphology across the frequency axis. A selection of these signals is shown in Supplementary Fig. 9.

We can conclusively state that all lookalike and mirrored lookalike signals are RFI due to their appearance in off-source observations.

Characterizing the blc1 lookalike population. The presence of this population of both positively and negatively sloped blc1 lookalikes preliminarily suggests that all lookalikes (including blc1) share a common origin. We can further assess this claim by examining the similarity in the parametric distributions of the lookalike signals and of blc1. We find that blc1 is consistent with the lookalike population in absolute drift rate, frequency and S/N (Fig. 4).

Determining the origin of the blc1 lookalike population. We can further strengthen the claim that the lookalike population shares a common origin if we can identify a frequency-shifting instrumental or electronic effect in the data. One potential source of that effect is instrumental harmonic distortion, which can produce replicas of an original frequency f signal at $2f$, $3f$ and so on. Another potential source is intermodulation distortion, a superset to harmonic distortion, which can produce a near-arbitrarily complex sequence of replicas that are integer multiples of the sums and differences of two or more original signals.

Harmonic analysis. We investigated whether any of the positive-drift lookalikes could be linked via a harmonic sequence. We generated the first 20 harmonics of a range of fundamental frequencies starting outside the bandpass at 100 MHz and progressing to 1,000 MHz in 1 kHz intervals. We defined a potential ‘harmonic sequence’ within the data as a set of two or more lookalikes (blc1 included) associated by the same fundamental frequency, within 1 kHz of their theoretical values. The blc1 signal was not consistent with being in a harmonic sequence with any of the observed lookalikes. However, a harmonic sequence did interlink a set of other lookalikes (Supplementary Table 2). This harmonic sequence contained frequencies of the form $n + 0.1m + 0.099$ MHz, where m and n are integers; because of the constant term, we refer to this set as ‘x.y99’.

Intermodulation analysis. Some lookalikes showed additional frequency structure that was not present in blc1. Two sets of lookalikes, which we will refer to as ‘triple feature’ (TF) and ‘single feature’ (SF), were distinguishable from their morphology alone. An example from the TF set is shown in Supplementary Fig. 10. TF and SF contained both positive lookalikes and mirrored lookalikes. TF had spacings that were integer multiples of 133.33 MHz. SF had a more complicated relationship of spacings, primarily integer multiples of 15 MHz but with an additional appearance of 128 MHz. In all cases within both sets, these frequencies are consistent with common clock oscillator frequencies used in digital electronics, with matches within 1–1,000 Hz of the expected value.

The three initially identified sets, namely TF, SF and the harmonic ‘x.y99’ set (see ‘Harmonic analysis’), each have a transition region in which the morphology of the signal flips, with positive lookalikes on one side and mirrored lookalikes on the other (Supplementary Fig. 11). If intermodulation effects were present, we predicted that we should detect a strong, zero-drift interferer at a frequency within the transition region, whose position is dictated by clock oscillator frequencies previously identified in the set.

For TF, we find a strong interferer at the predicted central frequency of 1,400 MHz, consistent to a single channel (± 4 Hz). For SF, one central frequency consistent with the 30 MHz spacing is 1,200 MHz, where we also see a strong interferer consistent at the Hz level. For x.y99, we predict a central frequency of 1,332 MHz but see only an extremely faint interferer; we do see strong signals

at 1,330.0000 MHz, 1,331.2000 MHz and 1,332.1805 MHz. This inconsistency could be caused by additional transposition (from an additional oscillator) present within the set, implying that one of the three listed frequencies is actually the responsible interferer. We conclude that these intentional-seeming separations seem likely to have been produced by the intermodulation of at least one clock oscillator with a strong interferer.

We found evidence for additional clock oscillator frequencies affecting the lookalike population, including the sets displayed in Fig. 5. As shown in Fig. 5a, we searched for patterns with integer kHz offsets (as in ‘Harmonic analysis’) and uncovered two individual sequences with spacings consistent with a 2.000004 MHz clock oscillator. Our data have a resolution of ~ 4 Hz, so we expect that the last digit has an error of ± 4 , which will propagate in the integer multiplication of spacings. In Fig. 5 we display the extra error at the Hz level to illustrate that these spacings are clearly the product of the same oscillator: not only are the general spacings consistent with powers of 2.000004 MHz, but the errors on those spacings are consistent with propagating errors on the order of ± 4 Hz, for example, 16.000038 MHz. In Fig. 5b, we see these exact spacings relating blc1 (within propagated error, on the order of 100 Hz) with three lookalikes at ~ 712 MHz, ~ 856 MHz and $\sim 1,062$ MHz.

This numerical analysis indicates that blc1 is an intermodulation product produced by a ~ 2 MHz clock oscillator that is mixed with some other zero-drift RFI elsewhere in the band. We also find that power at the blc1-companion lookalike frequencies from Fig. 5 is detected when the four archival signals at 982.002 MHz are detected, just like blc1, and is not detected when the archival signals are not present (Supplementary Discussion 1.4).

This interpretation provides an explanation for the appearance of the signal in a part of the spectrum reserved for aviation and navigation: the source was not intending to transmit in that frequency region, and the signal was instead generated by the interaction of electronics within the transmitter, the receiver or both. In this case, the underlying signals that intermodulate to cause the lookalikes are likely from outside Murriyang’s receiver system. Signals are digitized using three analogue-to-digital cards inside the telescope focus cabin, with further processing done in radio-frequency-tight cabinets in the telescope tower⁶. As the lookalikes span across all three analogue-to-digital cards, they are unlikely to be spurious signals generated within the receiver’s digital systems.

The blc1 signal cannot be the original signal because it is two orders of magnitude weaker than the strongest signals in the set and is not seen in the off-panels, which is not replicated across the set. Evidently, blc1’s duty cycle or variability tracks the observing cadence on ProxCen, leading to the apparent localization on the sky. If blc1 were always ‘on’ at its brightest power, it would have been detected in all off-sources. Supplementary Figs. 7 and 9 reveal a range of inter-panel brightness behaviours for the lookalikes; some appeared in every panel, whereas some were as faint as blc1 and missing from all but the first panel. By the thresholding and on-off selection mechanisms, turboSETI selected the most interesting signal from a set of potentially hundreds of intermodulation products. These large numbers speak to the particular pathology of this case, as this behaviour had never been seen in over a year of UWL observations.

RFI environment analysis is unfortunately complex, and the RFI environment around most astronomical radio facilities

Fig. 3 | A waterfall plot around 982 MHz depicting a signal similar to blc1 that occurred on 2019 April 30. The signal is the bright sloping feature, but is clearly overlaid on a non-drifting, comb-like signal (see ‘Frequency comb’). Both the signal and the comb underneath seem to be RFI as they appear in the off-source observations. In Supplementary Table 1, we derived the S/N, drift rate and start frequency of each panel of the blc1 observation; we derived the properties of this signal in the same manner (Supplementary Methods 2.1). The drift rate (median 0.021 Hz s^{-1}), S/N (median 6.9) and frequency range (982.0021–982.0023 MHz) are consistent with those of blc1, and this signal is also unresolved.

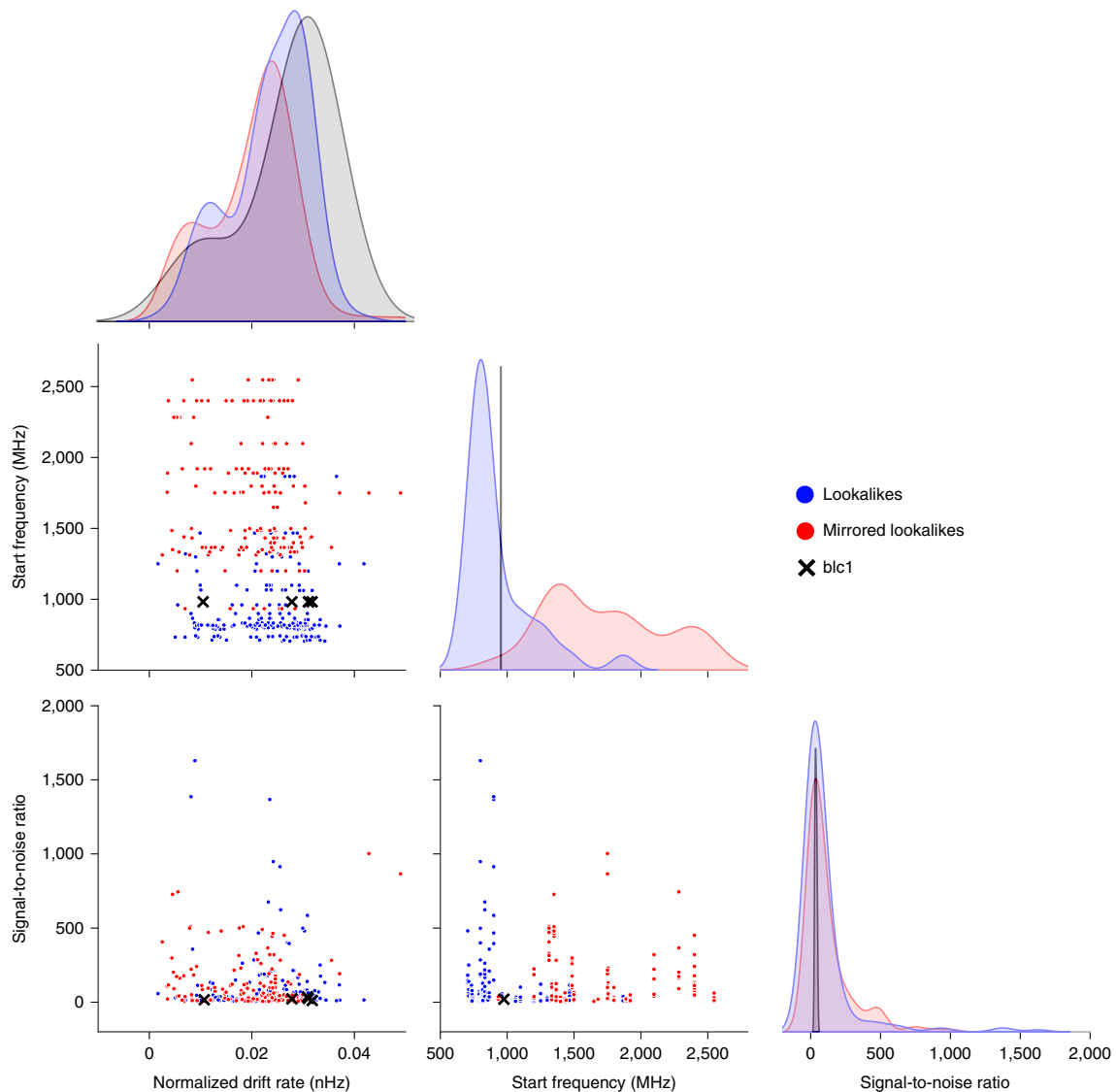


Fig. 4 | A corner plot showing the population of lookalikes and mirrored lookalikes compared to b1c1 in start frequency, normalized drift rate and signal-to-noise ratio. For the mirrored lookalikes, which have negative normalized drift rates, we took the absolute value for comparison. The heights of the kernel density estimations are not to scale, as the population of b1c1 points is so much smaller than the other two populations that it would otherwise not be visible on these axes. The b1c1 signal (x symbols and grey shading) is consistent with the signal-to-noise and normalized drift rate distributions (blue dots and shading for lookalikes, and red dots and shading for mirrored lookalikes) and, although slightly higher in frequency than the peak of the kernel density estimations for the lookalike population, is still consistent with that distribution.

is not well characterized at the frequency resolutions used for the SETI work. In the case of b1c1, the situation is more complicated still, with mixing products that obscure the frequency and character of the original, individual interferers. It is possible that we could untangle the origins of this interference. However, as the goal of this study was to determine whether b1c1 had an Earth-based or interstellar origin, we find that this is appropriate for future work.

Creation of a technosignature verification framework

The b1c1 signal is the first signal of interest from the Breakthrough Listen programme that required extensive signal verification to be undertaken. This case study led to a novel signal verification ‘tool-kit’ for future SETI signals of interest. Similar frameworks have been applied to searches for fast radio bursts¹⁹ and gravitational waves (for example, ref. ²⁰), but previous SETI programmes relied heavily

on re-observation alone without the application of a thorough checklist (for example, refs. ^{21,22}). We propose the following verification checks for narrowband technosignature signals of interest, once known astrophysical origins have been ruled out:

1. Verify that all instrumentation was functioning correctly.
2. Verify that the signal of interest was not present in the off-source observations at a lower S/N threshold.
3. Check for catalogued RFI at the same frequency at the observatory where the signal of interest was discovered.
4. Compare the drift rate evolution of the signal of interest to known accelerational and electronic drifts from human-made technology.
5. Compare the drift rate evolution of the signal of interest to the expected drift rates and periods in the target system and the Solar System.

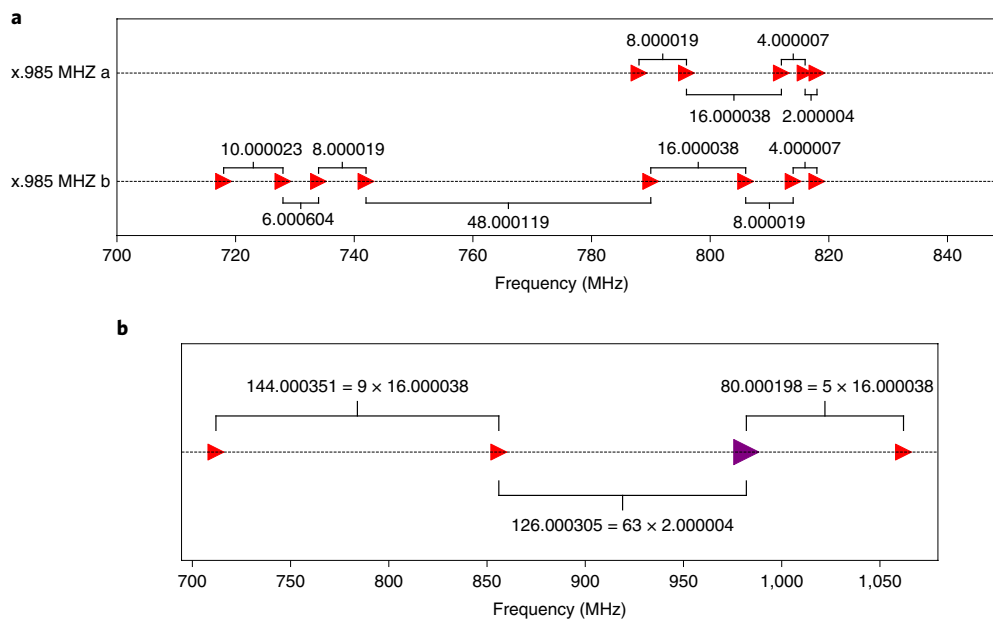


Fig. 5 | A visualization of 16 signals from the lookalike set and b1c1, divided into three sets. a, Two sets of positive lookalikes found within the data, originally identified by their position at 985 kHz above an integer MHz in each appearance. The full spacings, to Hz precision, are shown to demonstrate the set's consistency with mixing from a 2.000004 MHz clock oscillator. Recall that the spacings have an inherent, multiplicative ± 4 Hz error from the discrete frequency resolution. One spacing that we see in both sets, apparently resulting from this same oscillator, is 16.000038 MHz. The two sets are both affected by the same oscillator, but they are not consistent with each other to a multiple of 2.000004 MHz, illustrating another complexity within the data set. **b**, The b1c1 signal (purple) shown in sequence with three additional lookalikes (red), which are consistent with integer multiples of 2.000004 MHz, including exactly 16.000038 MHz; this set of clock-oscillator-induced spacings is perfectly consistent with the spacings uncovered in the sets in **a**.

- Search for other potential instances of the signal of interest in archival data from the same observatory.
- Search for similar signals at other frequencies within the observation in which the signal of interest was detected. If found, determine whether these signals have characteristics consistent with RFI.
- Qualitatively or, if possible, quantitatively assess whether similar signals (from Steps 6 and 7 above) are generated by the same phenomenon as the signal of interest.
- If other signals are indeed from the same phenomenon as the signal of interest, determine whether they are RFI using the off-source observations or, if necessary, Steps 1–8.
- Re-observe the target with both the same instrument and other instruments to attempt to re-detect the signal of interest.

The checklist as written is appropriate for persistent, narrowband technosignature searches with single-beam, single-dish telescopes. The procedure can be applied to multi-beam instruments by using other beams as 'reference pixels' for the on-source beam, instead of nodding to an off-source position. In addition, re-observation (Step 10) may be performed earlier in the checklist if economical, especially in cases in which the signal of interest would be expected to be periodic or transient on long timescales (that is, synchronized with the transit of an exoplanet).

Future work

The b1c1 signal has underscored that, when practicable, simultaneous observations of potential technosignatures should be conducted at two different observing sites simultaneously. For ProxCen, simultaneous observing could be accomplished with MeerKAT (for example, ref. ²³) and Murriyang, whose receivers share a frequency overlap of about 1 GHz including the 982 MHz region of b1c1. There is a ~ 4.5 h window during which the source can be observed

simultaneously at the two sites. Although re-observations are resource-intensive, they are also scientifically meritorious in their own right. ProxCen is still a uniquely fascinating SETI target for all of the reasons described in the Introduction, and it will become even better characterized by future astrobiology-oriented studies.

We are also investigating other ways to further characterize b1c1 in both the hardware and software components of the pipeline. Other Murriyang observers are monitoring for interference near 982 MHz, which could help us identify position-dependent RFI. To characterize aliasing behaviour within the receiver, the sky signal could be excluded by covering the feed with cryogenically cooled radio-frequency-absorbing material that can be treated as a thermal blackbody (known as a 'cold load'). This poses engineering and logistical challenges, but may allow us to identify the different components whose mixing produces the intermodulation product at 982 MHz. To understand the particular pathology of variability patterns such as those of b1c1, we could perform noise-injection testing on the lookalike population. Finally, this case study implies that taking data during slews in future single-dish SETI observations could help us better understand signal localization and sidelobe behaviour in future programmes.

The impact of b1c1

Although we attribute b1c1 to RFI, the benefits from its unique analysis will inform searches for years to come. This paper outlines a 'checklist' that provides thorough next steps for this type of signal. We have developed new software that will be incorporated into BL's analysis packages (for example, blimpy and turboSETI), such that future signals of interest can be assessed more quickly and efficiently.

The detection of b1c1 shows the success of the BL signal detection pipeline. From 26 h of observations over billions of channels, the turboSETI algorithm was able to retrieve a set of potential

signals of interest. The blc1 signal was then easily identified from this set upon visual inspection of the software outputs.

Conversely, this signal of interest also reveals some novel challenges with radio SETI validation. It is well understood within the community that single-dish, on-off cadence observing could lead to spurious signals of interest in the case in which the cadence matches the duty cycle of some local RFI. The blc1 signal provided the first observational example of that behaviour, albeit in a slightly different manner than expected (variation of signal strength over position and time, which changed for each lookalike within the set). This case study prompts further application of observing arrays, multi-site observing and multi-beam receivers for radio technosignature searches. For future single-dish observing, we have demonstrated the utility of a deep understanding of the local RFI environment. To gain this understanding, future projects could perform omnidirectional RFI scans at the observing site, record and process the data with instrumentation with high frequency resolution such as the various BL backends, and then use narrowband search software such as turboSETI to obtain a population with which to characterize the statistics (in frequency, drift, power, duty cycle and so on) of local RFI.

Finally, blc1 encourages us to continue working at logistical challenges that have traditionally vexed large radio SETI efforts. In a project with an incredibly high rate of data inflow, how do we work towards data analysis in real time? When raw voltage data are exceedingly memory-intensive to store, how do we decide pre-analysis which observations may need additional analysis in the raw voltage products? For example, one solution to the data-storage challenge is to store only 'postage stamps' of events with limited time and frequency ranges. Here we have learned that neglecting to consider the entire operable bandwidth of a receiver can have serious consequences, for example, losing the context that can be used to show that a signal of interest is RFI.

Data availability

All data used in this manuscript are stored as high-resolution filterbank files, which are available through the Breakthrough Listen Open Data Archive at <http://seti.berkeley.edu/opendata>. This includes all observations from the original observing campaign in 2019 April, as well as the re-observations in 2020 November, 2021 January and 2021 April.

Code availability

The software tools used to read these files (input/output) and perform the narrowband search are publicly available at <https://github.com/UCBerkeleySETI/blimpy> and at https://github.com/UCBerkeleySETI/turbo_seti.

Received: 3 March 2021; Accepted: 3 September 2021;

Published online: 25 October 2021

References

- Des Marais, D. et al. The NASA astrobiology roadmap. *Astrobiology* **8**, 715–730 (2008).
- van Leeuwen, F. Validation of the new Hipparcos reduction. *Astron. Astrophys.* **474**, 653–664 (2007).
- Anglada-Escudé, G. et al. A terrestrial planet candidate in a temperate orbit around Proxima Centauri. *Nature* **536**, 437–440 (2016).
- Suárez Mascareño, A. et al. Revisiting Proxima with ESPRESSO. *Astron. Astrophys.* **639**, A77 (2020).
- Worden, S. P., Drew, J. & Klupar, P. Philanthropic space science: the breakthrough initiatives. *New Space* **6**, 262–268 (2018).
- Hobbs, G. et al. An ultra-wide bandwidth (704 to 4 032 MHz) receiver for the Parkes radio telescope. *Publ. Astron. Soc. Aust.* **37**, e012 (2020).
- Zic, A. et al. A flare-type IV burst event from Proxima Centauri and implications for space weather. *Astrophys. J.* **905**, 23 (2020).
- Price, D. C. et al. The Breakthrough Listen search for intelligent life: wide-bandwidth digital instrumentation for the CSIRO Parkes 64-m telescope. *Publ. Astron. Soc. Aust.* **35**, e041 (2018).
- Price, D. C. et al. Expanded capability of the Breakthrough Listen Parkes data recorder for observations with the UWL receiver. *Res. Notes Amer. Astron. Soc.* **5**, 114 (2021).
- Lebofsky, M. et al. The Breakthrough Listen search for intelligent life: public data, formats, reduction, and archiving. *Publ. Astron. Soc. Pac.* **131**, 124505 (2019).
- Smith, S. et al. A radio technosignature search towards Proxima Centauri resulting in a signal of interest. *Nat. Astron.* <https://doi.org/10.1038/s41550-021-01479-w> (2021).
- Forgan, D. et al. Rio 2.0: revising the Rio scale for SETI detections. *Int. J. Astrobiology* **18**, 336–344 (2019).
- Tarter, J. The search for extraterrestrial intelligence (SETI). *Annu. Rev. Astron. Astrophys.* **39**, 511–548 (2001).
- Price, D. C. et al. The Breakthrough Listen search for intelligent life: observations of 1327 nearby stars over 1.10–3.45 GHz. *Astrophys. J.* **159**, 86 (2020).
- Enriquez, J. E. et al. The Breakthrough Listen search for intelligent life: 1.1–1.9 GHz observations of 692 nearby stars. *Astrophys. J.* **849**, 104 (2017).
- Wright, A. & Otrupcek, R. Parkes Catalog, 1990, Australia Telescope National Facility. *PKS Catalog* (1990).
- Perryman, M. et al. The HIPPARCOS catalogue. *Astron. Astrophys.* **323**, 49–52 (1997).
- Isaacson, H. et al. The Breakthrough Listen search for intelligent life: target selection of nearby stars and galaxies. *Publ. Astron. Soc. Pac.* **129**, 054501 (2017).
- Foster, G. et al. Verifying and reporting fast radio bursts. *Mon. Not. R. Astron. Soc.* **481**, 2612–2627 (2018).
- Abbott, B. P. et al. Observation of gravitational waves from a binary black hole merger. *Phys. Rev. Lett.* **116**, 061102 (2016).
- Horowitz, P. Project META: what have we found? *Planet. Rep.* **13**, 4–9 (1993).
- Anderson, D. et al. SETI@home: internet distributed computing for SETI. *Astron. Soc. Pac. Conf. Ser.* **213**, 511 (2000).
- Jonas, J. L. MeerKAT - The South African array with composite dishes and wide-band single pixel feeds. *Proc. IEEE* **97**, 1522–1530 (2009).

Acknowledgements

Breakthrough Listen is managed by the Breakthrough Initiatives, sponsored by the Breakthrough Prize Foundation. The Murrumbidgee radio telescope is part of the Australia Telescope National Facility, which is funded by the Australian government for operation as a national facility managed by CSIRO. We thank the staff at Murrumbidgee for their observational support. S.S. and S.C. were supported by the United States National Science Foundation under the Research Experience for Undergraduates programme at the Berkeley SETI Research Center site (grant no. 1950897). We thank R. Elkins and L. Cruz for help with development and debugging of turboSETI.

Author contributions

S.Z.S. led the data analysis and wrote the manuscript. S.S. and D.C.P. uncovered blc1 and analysed data. D.D. and B.C.L. ran simulations and analysed data. D.J.C., S.C., V.G., H.I., M.L., D.H.E.M., C.N., K.I.P., A.V.P.S. and C.I.W. assisted with data analysis, scientific interpretation and manuscript revision. A.Z. obtained the data via commensal observing. J.D. and S.P.W. reviewed the manuscript.

Competing interests

The authors declare no competing interests.

Additional information

Supplementary information The online version contains supplementary material available at <https://doi.org/10.1038/s41550-021-01508-8>.

Correspondence and requests for materials should be addressed to Sofia Z. Sheikh.

Peer review information *Nature Astronomy* thanks Michael Garrett and the other, anonymous reviewer for their contribution to the peer review of this work.

Reprints and permissions information is available at www.nature.com/reprints.

Publisher's note Springer Nature remains neutral with regard to jurisdictional claims in published maps and institutional affiliations.



Open Access This article is licensed under a Creative Commons Attribution 4.0 International License, which permits use, sharing, adaptation, distribution and reproduction in any medium or format, as long as you give appropriate credit to the original author(s) and the source, provide a link to the Creative Commons license, and indicate if changes were made. The images or other third party material in this article are included in the article's Creative Commons license, unless indicated otherwise in a credit line to the material. If material is not included in the article's Creative Commons license and your intended use is not permitted by statutory regulation or exceeds the permitted use, you will need to obtain permission directly from the copyright holder. To view a copy of this license, visit <http://creativecommons.org/licenses/by/4.0/>.

© The Author(s) 2021